GREEN SYNTHESIS OF Fe_2O_3 NANOPARTICLES USING *OLEA EUROPAEA* LEAF EXTRACT AND THEIR ANTIBACTERIAL ACTIVITY

A. M. MOHAMMED[*], W. M. SAUD, M. M. ALI
Department of Chemistry, College of Science, University Of Anbar, Ramadi, Iraq

Fe_2O_3 nanoparticles (NPs) were prepared using *Olea europaea* leaf extract. The structure and size of Fe_2O_3 NPs were analyzed through transmission electron microscopy, field emission scanning electron microscopy, X-ray diffraction, and atomic force microscopy. This study investigated the significant difference in the activities of some antibiotics, such as cefixime, levofloxacin, amikacin, norflexin, trimethoprim, doxycycline, and gentamicin against *Klebsiella pneumoniae* and compared their synergistic effects with Fe_2O_3 NPs. The inhibition zone of cefixime increased from 283 mm^2 to 17490, 314, and 314 mm^2 when it was mixed with Fe_2O_3 NPs, the inhibition zone of levofloxacin increased from 113.04 mm^2 to 254.34, 200.96, and 153.86 mm^2 using concentrations (3200, 2000, 1000) ppm of Fe_2O_3 NPs.

1. Introduction

Metal nanoparticles (NPs), such as Ag, Au, Fe, and Pd, have been widely investigated in several fields, such as physics [1], chemistry [2], medicine [3], and biology [4] because of their different properties in their bulk state [5]. Metal NPs have been widely applied in sensing [6], biomedicine [7,8], catalysis [9], fuel cells [10], photonics [11], and electronics [12]. The synthesis of metal NPs involves the reduction of a metal salt using mechanical, physical, biological, and chemical methods. Biogenic substances, such as microbes and plant extracts, are used as reducing agents to these metal salts because they are cost-effective, eco-friendly, and simple. Biomolecules existing in plant extracts, such as carbohydrates, steroids, and flavonoids, work as reducing and capping agents because they act as phyto constituents, thereby ensuring the stability of NPs [13].

Iron oxides involve many forms, such as α-Fe_2O_3, β-Fe_2O_3, γ-Fe_2O_3, Fe_3O_4, and Fe-Fe_2O_3 [14,15]. α-Fe_2O_3 is considered the stable phase and common form of iron oxides, where Fe_2O_3 (hematite) NPs have attracted major interest in biomedical applications [16] and gas sensors [17].

α-Fe_2O_3 is a canted antiferromagnetic, γ-Fe_2O_3 is a paramagnetic, and β-Fe_2O_3 is a ferromagnetic material. The magnetic moment of α-Fe_2O_3 is smaller (~1 emu/cc) compared with the magnetic moment of γ-Fe_2O_3 (~430 emu/cc).

Iron oxide NPs have been widely used by scientists in magnetic particle imaging [18], bio magnetic testing, and delivery of targeted drugs [19-21].

The ability of iron oxides to produce heat in a magnetic field makes them suitable for hyperthermia applications. Iron oxides are involved in many applications, such as medicine, chemical industry, and water purification [22]. Iron oxide NPs are used in biocompatibility applications and are considered active substances against bacteria and cancer tumors [23,24]. Iron oxide NPs also reduce and prevent the cell membrane formation of pathogenic bacteria, thereby making them important in medical instruments. Iron oxide NPs represent substances that are resistant to the growth of microorganisms, and are used as antibacterial because of their ability to receive biocompatible coating, super para magnetism, and small size (10–30 nm) [25].

Iron oxide NPs inhibit glycocalyx formation to prevent bacterial growth [26]. This process is important for inhibiting bacterial adhesion on medical devices. α-Fe_2O_3 NPs, including nanowires, hollow spheres, nanotubes, and nano flowers, have various morphologies [27]. The

---

[*] Corresponding author: sc.dr.ahmedm.mohammed@uoanbar.edu.iq

liquid phase is widely used to prepare α-Fe_2O_3 NPs because of its unique features, simple equipment, and simple operation.

Different manufacturing methods have been developed to prepare iron oxide NPs with the required properties. These methods include physical (such as irradiation by UV radiation) [28], chemical [29], co-precipitation [30], thermal decomposition [31], and biological or green methods [32]. The green method is a useful method for with high-quality output and low cost. However, this method requires longer time period than that of physical and chemical methods, as shown in Fig. 1.

Fig. 1. Green synthesis nanotechnology.

This study aims to provide a robust synthesis protocol for the formation of iron oxide NPs with a narrow size distribution and contribute to understanding the mechanism of synthesis and growth of iron oxide NPs by investigating their properties. The effects of these NPs on bacteria are assessed, and their amounts of inhibitory effect are determined.

2. Materials and methods

2.1. Materials
In this study, *Olea europaea* leaves were collected from *O. europaea* trees at the University of Anbar, Ramadi, Iraq, as shown in Figure 2. Iron (II) chloride tetra hydrate ($FeCl_2.4H_2O$) and iron (III) chloride hexa hydrate ($FeCl_3.6H_2O$) were purchased from Sigma-Aldrich. All chemicals were used without purification.

Fig. 2. View of olea europaea leaves.

2.2. Methods
2.2.1. Synthesis of O. europaea leaf extract
The taken leaves were carefully rinsed several times with distilled water in order to remove the dusts and were dried out at room temperature to remove the residual wetness and dampness. Then, the dry leaves were grinded into small pieces and finally powdered. Small pieces of *O. europaea* leaves (5 g) were placed in a flask with 500 mL sterile distilled water and heated in a water bath at 60 °C for 2 h. Then, the extract was cooled at room temperature before vacuum filtering using whatman filter paper No. 1 to obtain the extract. The extract was stored at 4 °C before synthesizing iron oxide NPs.

2.2.2. Synthesis of Fe₂O₃ NPs

Iron oxide NPs were synthesized by dissolving 1.20 g of $FeCl_3.6H_2O$ and 0.50 g of $FeCl_2.4H_2O$ with (1:2 molar ratio) in 100 mL of double distilled water in a 250 mL beaker and heated to 80 °C under mild stirring for 10 min. Then, 20 mL of aqueous solution of *O. europaea* leaf extract was slowly added into the resulting mixture. The light green color of *O. europaea* extract mixture changed to dark brown. After 10 min, 20 mL aqueous solution of sodium hydroxide was added to the mixtures at a rate of 3 mL/min to allow uniform precipitation of iron oxide. The mixture was cooled to room temperature, and iron oxide NPs were obtained through decantation to form magnetites. The formed magnetites were washed thrice with double distilled water and ethanol and air-dried at room temperature.

2.2.3. Characterization of iron oxide NPs

The particle size of iron oxide NPs was measured through transmission electron microscopy (TEM), field emission scanning electron microscopy (FE-SEM), and atomic force microscopy (AFM) (SPM-AA3000, Angstrom Advanced Inc., USA) under AFM contact mode. The structure and crystalline size of NPs were determined through X-ray diffraction (XRD) using an automated diffraction meter Shimadzu 6000 XRD with Cu-Kα radiation ($\lambda = 1.5418$ Å).

2.3. Diagnosis of isolation

Klebsiella pneumoniae (*K. pneumoniae*) isolates were obtained from microbiology laboratories at the Faculty of Science, University of Anbar, and isolation was confirmed by performing some biochemical tests, including the growth of nutritious broth and MacConkey agar, Gram staining, and diagnosis on VITEK 2.

2.4. Antibiotic sensitivity test

Various antibiotics, which are obtained from Bio Analyses Company, were spreading around the tables on Mueller Hinton agar fertilized with *K*. *pneumoniae* bacteria.

3. Result and discussion

3.1. TEM

TEM images shows the morphologies of Fe₂O₃ NPs, as shown in Fig. 3, where the size of prepared NPs using *O. europaea* leaf extract at 80 °C ranges from 50 nm to 60 nm. These particles have granule spherical shapes with small sizes, and their size depends on the amount of extract used during the synthesis of Fe₂O₃ NPs.
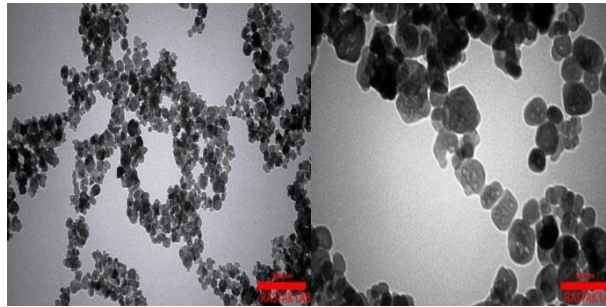
Fig. 3. TEM of Fe$_2$O$_3$ NPS green synthesis using europaea leaves extract with diameter of Fe$_2$O$_3$ NPS is around 50-60 nm and different magnification.

3.2. FE-SEM

The Fe$_2$O$_3$ has been synthesized, the surface morphologies were assessed using field emission scanning electron microscopy. The image resolution was processed using FE- SEM software and then presented as shown in Fig. 4. It can be clearly seen that the sample has spherical-like shape with uniform size distribution. Furthermore, the elemental compositions of as-synthesized Fe$_2$O$_3$ nano particles were analyzed through EDX spectra as shown in the Fig. 5. The spectra showed that the as-prepared nanoparticles comprise mainly of iron and oxygen. No other peaks related to impurities have been assigned in the spectra which confirm the purity of the iron oxide nanoparticles.
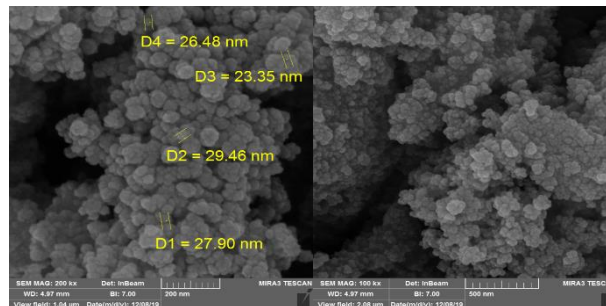
Fig. 4. FE-SEM image of Fe$_2$O$_3$ NPS.
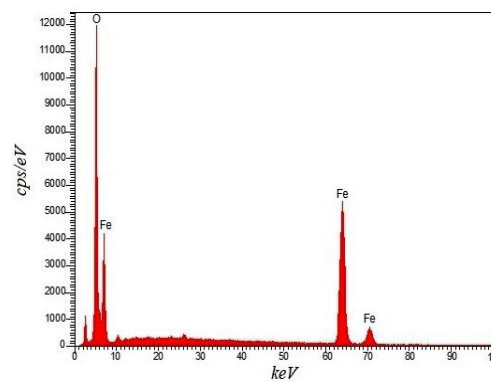
Fig. 5. EDX spectrum of Fe$_2$O$_3$ NPS.

3.3. AFM

The materials produced were confirmed as NPs through AFM. The results showed that the diameters of iron oxide NPs are 50 nm. The largest diameter of NPs was 60 nm. Fig. 6 represents the morphological characteristics and other properties (e.g., surface texture) of Fe_2O_3 NPs. The 2D and 3D shapes of the surface structure of Fe_2O_3 NPs are shown in Fig. 6. The results of AFM analysis were confirmed on the basis of the data gained using XRD.
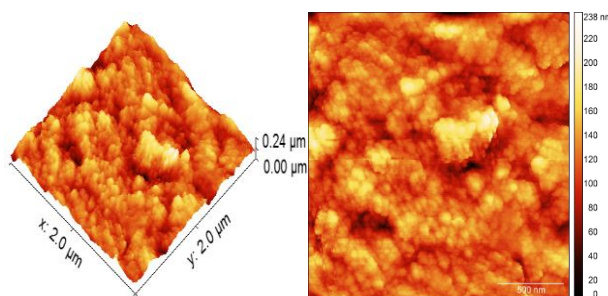
Fig. 6. AFM image of 2-dimensional and 3-dimensional of Fe_2O_3 NPS.

3.4. XRD analysis

The XRD pattern of the prepared iron oxide NPs using *O. europaea* extract is shown in Fig. 7. The strong characteristic peaks of iron oxide particles are obtained at 2θ = 24.13, 33.15, 35.61, 40.85, 49.47, 54.08, 62.44, and 63.98, which correspond to amorphous structures (012), (104), (110), (113), (024), (116), (214), and (300) of iron oxide, as shown in Table (1). All the reflection peaks could be indexed to the rhombohedral structure of iron oxide (JCPDS NO. 00-033-0664). These findings are analogous with the crystalline nature of iron oxide NPs [33].
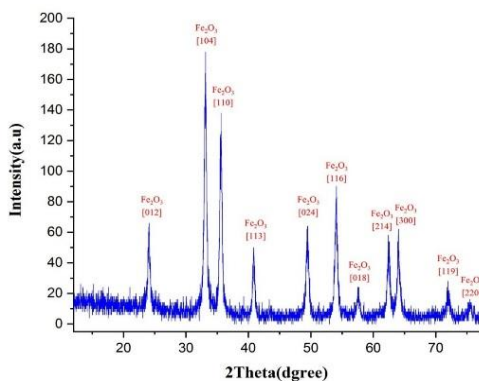
Fig. 7. XRD patterns of iron oxide nanoparticles synthesized by olea europaea extract.

Table 1. The structural parameters of Fe_2O_3 NPS as obtained from XRD analysis.

	2θ (degree)	
hk1	Observed	JCPDS
012	24.13°	24.14°
104	33.15°	33.14°
110	35.61°	35.61°
113	40.85°	40.84°
024	49.47°	49.45°
116	54.08°	54.06°
214	62.44°	62.42°
300	63.98°	64.00°

3.5. Antimicrobial activity

In this study, Fe_2O_3 NPs were evaluated in terms of their bactericidal potential against *K. pneumoniae*. Colloidal Fe_2O_3 NPs (10 µL) were injected into the media containing antibiotics. Bacteria were cultured in plates and incubated for 18-24 h at 37 °C. The inhibition zone diameter was measured using a ruler, and the result was compared with the antibiotics and Fe_2O_3 NPs as the control group. Fe_2O_3 NPs have been widely used in many fields, especially in medicine. In this research, the synthesized Fe_2O_3 NPs were applied as antibacterial agent via using a well diffusion assay. Fe_2O_3 NPs have antibacterial properties against *K. pneumoniae*. The growth of *K. pneumoniae* was inhibited using different types of antibiotics combined with the synthesized Fe_2O_3 NPs. The increase in evacuated spaces was significant with the combination of Fe_2O_3 NPs and antibiotics, as presented in Table 2.

Table 2. Area of inhibition zones for K. pneumoniae growth by using Fe₂O₃ NPS with antibiotics.

Anti-biotitic	Area of inhibition (mm^2) with Fe_2O_3 NPS (3200 ppm)	Area of inhibition (mm^2) with Fe_2O_3 NPS (2000 ppm)	Area of inhibition (mm^2) with Fe_2O_3 NPS (1000 ppm)	Area of inhibition (mm^2) without Fe_2O_3
(Cefixime) CFM	17490	314	314	283
(Trimethoprim) TMP	150	12.56	19.625	0
(Ampicillin) AM	915	63.585	12.56	12.56
(Levofloxacin) LEV	254.34	200.96	153.86	113.04
(Gentamicin) CN	132.665	94.985	38.465	19.625
(Augmeentin) AMC	10000	200.96	254.34	0
(Amikacin) AK	5220	452.16	283.385	176.625
(Norflexin) NOR	256	19.625	28.26	7.065
(Doxycycline) DO	915	50.24	78.5	0
(Ceftriaxone) CRO	20736	314	452.16	314

The increased inhibition zone has synergistic properties between antibiotics and Fe_2O_3 NPs. The biosynthesized Fe_2O_3 NPs have a necessary agent against microbes. They showed antibacterial activity in a concentration-dependent manner, where high concentrations exhibit large inhibition zone. The inhibition zone was 283 mm^2 when cefixime was used and increased to 17,490 mm^2 with the addition of Fe_2O_3 NPs (3200 ppm) against *K. pneumoniae,* as shown in Fig. 8.
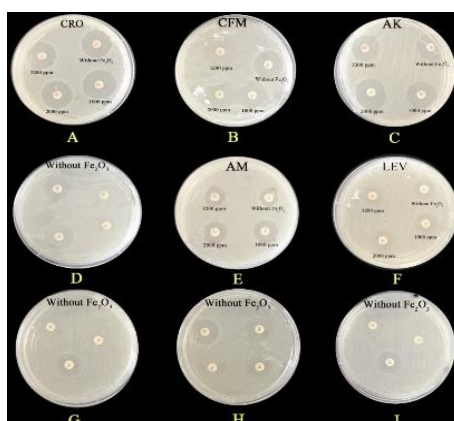
Fig. 8. Antibiotics with Fe$_2$O$_3$ NPS and antibiotics without Fe$_2$O$_3$ for inhibition zones K. pneumoniae growth.

Most antibiotics exhibit behavior similar to that of iron oxide nanoparticles, but with varying efficacy, CFM > CRO > AMC > AK > DO. as Fig 9.
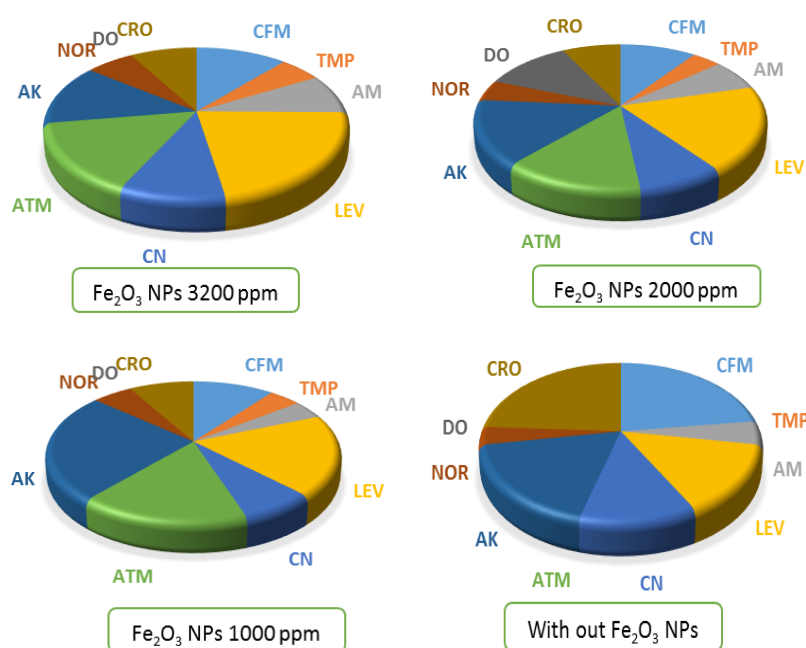
Fig. 9. Inhibition zones s for K. pneumoniae growth by using Fe$_2$O$_3$ NPS with antibiotics.

High concentrations of iron oxide NPs are more efficient in inhibiting the growth of *K. pneumoniae* than that of low concentrations on the basis of the synergistic effect of antibiotics. Similar mechanism was observed for positively charged NPs against various bacterial strains. However, the exact molecular nature of antibacterial action of Fe$_2$O$_3$ NPs remains to be elucidated [34].

4. Conclusions

This study investigated the effectiveness of biological method using *O. europaea* leaf extract to obtain iron oxide NPs with small particle sizes (50-60 nm). Fe_2O_3 NPs have strong antibacterial capabilities by combining with different types of antibiotics, such as levofloxacin, ceftriaxone, trimethoprim, cefixime, augmentin, norflexin, and doxycycline, and have many activities against *K. pneumoniae*.

Increasing the concentration of Fe_2O_3 NPs increases the inhibition area compared with antibiotics alone. High concentrations of iron oxide NPs are more efficient in inhibiting the growth of *K. pneumoniae* than that of low concentrations of Fe_2O_3 NPs. The antibacterial activity of Fe_2O_3 NPs depends on the concentrations, thereby exhibiting large inhibition zones.

References

[1] N. Basavegowda, K. Mishra, Y. R. Lee, Advances in Natural Sciences: Nanoscience and Nanotechnology **8**(2), 025017 (2017).
[2] W. Liu, A. K. Herrmann, N. C. Bigall, P. Rodriguez, D. Wen, M. Oezaslan, A. Eychmüller, Accounts of chemical research **48**(2), 154 (2015).
[3] M. Rai, A. P. Ingle, S. Birla, A. Yadav, C. A. D. Santos, Critical reviews in microbiology **42**(5), 696 (2016).
[4] M. Rai, A. P. Ingle, I. Gupta, A. Brandelli, International journal of pharmaceutics **496**(2), 159 (2015).
[5] M. B. Ross, J. C. Ku, V. M. Vaccarezza, G. C. Schatz, C. A. Mirkin, Nature nanotechnology **10**(5), 453 (2015).
[6] K. Saha, S. S. Agasti, C. Kim, X. Li, V. M. Rotello, Chemical reviews **112**(5), 2739 (2012).
[7] S. M. Gavade, G. H. Nikam, R. S. Dhabbe, S. R. Sabale, B. V. Tamhankar, G. N. Mulik, Advances in Natural Sciences: Nanoscience and Nanotechnology **6**(4), 045015 (2015).
[8] A. Ebrahiminezhad, M. Bagheri, S. M. Taghizadeh, A. Berenjian, Y. Ghasemi, Advances in Natural Sciences: Nanoscience and Nanotechnology **7**(1), 015018 (2016).
[9] V. A. Kumar, T. Uchida, T. Mizuki, Y. Nakajima, Y. Katsube, T. Hanajiri, T. Maekawa, Advances in Natural Sciences: Nanoscience and Nanotechnology **7**(1), 015002 (2016).
[10] S. Guo, E. Wang, Nano Today **6**(3), 240 (2011).
[11] C. Gong, M. S. Leite, ACS Photonics **3**(4), 507 (2016).
[12] E. Abbasi, M. Milani, A. S. Fekri, M. Kouhi, A. Akbarzadeh, N. H. Tayefi, M. Samiei, Critical reviews in microbiology **42**(2), 173 (2016).
[13] S. Ahmed, M. Ahmad, B. L. Swami, S. Ikram, Journal of advanced research **7**(1), 17 (2016).
[14] S. K. Maji, N. Mukherjee, A. Mondal, B. Adhikary, Polyhedron **33**(1), 145 (2012).
[15] S. Upadhyay, K. Parekh, B. Pandey, Journal of Alloys and Compounds **678**, 478 (2016).
[16] S. Cabanas-Polo, M. Distaso, W. Peukert, A. R. Boccaccini, Journal of nanoscience and nanotechnology **15**(12), 10149 (2015).
[17] S. Liang, J. Li, F. Wang, J. Qin, X. Lai, X. Jiang, Sensors and Actuators B: Chemical **238**, 923 (2017).
[18] V. C. Karade, S. B. Parit, V. V. Dawkar, R. S. Devan, R. J. Choudhary, V. V. Kedge, A. D. Chougale, Heliyon **5**(7), 02044 (2019).
[19] P. B. Patil, V. C. Karade, P. P. Waifalkar, S. C. Sahoo, P. Kollu, M. S. Nimbalkar, P. S. Patil, IEEE Transactions on Magnetics **53**(11), 1 (2017).
[20] V. C. Karade, P. P. Waifalkar, T. D. Dongle, S. C. Sahoo, P. Kollu, P. S. Patil, P. B. Patil, Materials Research Express **4**(9), 096102 (2017).
[21] L. H. Reddy, J. L. Arias, J. Nicolas, P. Couvreur, Chemical reviews **112**(11), 5818 (2012).
[22] A. Lassoued, B. Dkhil, A. Gadri, S. Ammar, Results in physics **7**, 3007 (2017).
[23] R. Thomas, I. K. Park, Y. Y. Jeong, International journal of molecular sciences **14**(8), 15910 (2013).
[24] A. Marcu, S. Pop, F. Dumitrache, M. Mocanu, C. M. Niculite, M. Gherghiceanu, C. Grigoriu, Applied Surface Science **281**, 60 (2013).

[25] I. M. Hamouda, Journal of biomedical research **26**(3), 143 (2012).

[26] H. T. AL-Mousawi, M. I. AL-Taee, M. N. Rasheed, Q. N. AL-Hajjar, Iraqi Journal of Biotechnology **18**(2), 201 (2019).

[27] A. Rufus, N. Sreeju, D. Philip, RSC Advances **6**(96), 94206 (2016).

[28] J. Xie, Z. Zhou, Y. Lian, Y. Hao, P. Li, Y. Wei, Ceramics International **41**(2), 2622 (2015).

[29] D. Ling, N. Lee, T. Hyeon, Accounts of chemical research **48**(5), 1276 (2015).

[30] S. J. Mohammad, F. A. Rasin, Iraqi Journal of Science Part A, 106 (2016).

[31] R. Hufschmid, H. Arami, R. M. Ferguson, M. Gonzales, E. Teeman, L. N. Brush, K. M. Krishnan, Nanoscale 7(25), 11142 (2015).

[32] S. Saif, A. Tahir, Y. Chen, Nanomaterials **6**(11), 209 (2016).

[33] B. Yu, Journal of Materials Chemistry **20**(38), 8320 (2010).

[34] A. O. Shakeel, S. A. Rukhsana, I. A. Syed, Z. Polish Journal of Chemical Technology **19**(10), 110 (2017).